Experimental Determination of the Spin Density in the Tetracyanoethenide Free Radical, [TCNE]$^{\bullet -}$, by Single-Crystal Polarized Neutron Diffraction. A View of a π^* Orbital

Andrey Zheludev,[1a] André Grand,[1b] Eric Ressouche,[1a] Jacques Schweizer,*[,1a] Brian G. Morin,[1c] Arthur J. Epstein,*[,1c,d] David A. Dixon,*[,1e] and Joel S. Miller*[1e,f]

Contribution from the DRFMC/SPSMS/CENG, 85X,38041 Grenoble, France, the Department of Physics and the Department of Chemistry, The Ohio State University, Columbus, Ohio 43210-1106, and the DuPont Science & Engineering Laboratories, Experimental Station, E-328, Wilmington, Delaware 19880-0328

Received December 20, 1993®

Abstract: Polarized single-crystal neutron diffraction studies of tetra-*n*-butylammonium tetracyanoethenide, $[Bu_4N]^+[TCNE]^{\bullet -}$, have been used to locate the spin distribution in $[TCNE]^{\bullet -}$, a key component of several molecule-based magnets. This result confirms that the singly occupied orbital of $[TCNE]^{\bullet -}$ is the π^* antibonding molecular orbital consistent with molecular orbital predictions. The results show that the spin density around the central sp^2-carbon atoms is bent away from the midpoint of the C–C bond; it is not centered over the carbon nuclei. The spin localized on the individual sp^2-C, sp-C, and N atoms is respectively 33%, –5%, and 13% of the total spin on the tetracyanoethenide radical. The experimental results are compared with the results from *ab initio* molecular orbital and density functional theory calculations. The best agreement with experiment is found at the density functional level with 29%, –4%, and 15% of the total spin on the sp^2-C, sp-C, and N atoms. These results provide a basis to ultimately understand the ferromagnetic spin-coupling mechanism of molecule-based magnets.

Introduction

The synthesis of molecule/organic-based magnetic solids with ordering (critical) temperatures, T_c, sufficiently high to be useful in commercial applications is an important challenge. Electron-transfer complexes possessing chains of alternating donors ($D^{\bullet +}$) and acceptors ($A^{\bullet -}$) have been particularly useful for achieving ferromagnetic coupling. An early discovery was that $[Fe(C_5Me_5)_2]^{\bullet +}[TCNE]^{\bullet -}$ (TCNE = tetracyanoethylene) is a ferromagnet with $T_c = 4.8$ K.[2] This solvent soluble salt is comprised of chains of alternating decamethylferrocenium cations and tetracyanoethenide anions, and each ion has an $S = {}^1/_2$ spin. Other successful syntheses also involve $[TCNE]^{\bullet -}$ and include ferromagnetic $[M(C_5Me_5)_2]^{\bullet +}[TCNE]^{\bullet -}$ [M = Mn,[3] Cr[4,5]] and ferrimagnetic $V[TCNE]_x{\cdot}yCH_2Cl_2$ ($T_c \sim 400$ K)[6] and $[MnTPP]^{\bullet +}[TCNE]^{\bullet -}$ (TPP = *meso*-tetraphenylporphine) ($T_c = 18$ K).[7] In these latter two structures, $[TCNE]^{\bullet -}$ coordinates directly to the metal ions.

In order to design new materials with higher T_c's it is important to understand the nature of the ferromagnetic coupling among the spin-containing moieties. This interaction is strongest within a chain; however, ferromagnetism is a true three-dimensional phenomenon. A simple model for describing the magnetic spin coupling is a McConnell mechanism.[8,9] This model has been subject to criticism[10] and other explanations include spin polarization of the C_5Me_5 ligands and their coupling with the spin density on $[TCNE]^{\bullet -}$.[10,11] According to Tchougreff[12] the net ferromagnetism for $[Fe(C_5Me_5)_2][TCNE]$ arises from ferromagnetic coupling of d-electrons of the cation with the electrons back-transferred from $[TCNE]^{\bullet -}$ to the empty orbitals of $[Fe(C_5Me_5)_2]^{\bullet +}$; thus the spin density on the C_5Me_5 rings is predicted to align with that on $[TCNE]^{\bullet -}$ and Fe^{III}. In contrast, the theory proposed by Kahn and co-workers predicts alternating spin densities for the $[TCNE]^{\bullet -}$–ligand–Fe^{III} system chain.[13] The McConnell configuration interaction mechanism has also been proposed[2,6d,14] for direct coupling between the V and $[TCNE]^{\bullet -}$.

* Abstract published in *Advance ACS Abstracts,* May 1, 1994.

(1) (a) DRFMC/SPSMS/CENG. (b) DRF/SESAM/CENG. (c) Department of Physics, The Ohio State University. (d) Department of Chemistry, The Ohio State University. (e) DuPont (Contribution No. 6619). (f) Current address: Department of Chemistry, University of Utah, Salt Lake City, UT 84112.

(2) Miller, J. S.; Epstein, A. J. *Angew Chem.* **1994**, *106*, 399; *Angew. Chem., Int. Ed. Engl.* **1994**, *33*, 385. Buchachenko, A. L. *Russ. Chem. Rev.* **1990**, *59*, 307. Buchachenko, A. L. *Usp. Khim.* **1990**, *59*, 529. Kahn, O. *Struct. Bonding* **1987**, *68*, 89. Kahn, O. In press. Caneschi, A.; Gatteschi, D.; Sessoli, R.; Rey, P. *Acc. Chem. Res.* **1989**, *22*, 392. Miller, J. S.; Epstein, A. J.; Reiff, W. M. *Acc. Chem. Res.* **1988**, *21*, 114. Miller, J. S.; Epstein, A. J.; Reiff, W. M. *Science* **1988**, *240*, 40. Miller, J. S.; Epstein, A. J. *New Aspects of Organic Chemistry*; Yoshida, Z., Shiba, T., Ohsiro, Y., Eds.; VCH Publishers: New York, 1989; p 237.

(3) Yee, G. T.; Manriquez, J. M.; Dixon, D. A.; McLean, R. S.; Groski, D. M.; Flippen, R. B.; Narayan, K. S.; Epstein, A. J.; Miller, J. S. *Adv. Mater.* **1991**, *3*, 309.

(4) Miller, J. S.; McLean, R. S.; Vazquez, C.; Calabrese, J. C.; Zuo, F.; Epstein, A. J. *J. Mater. Chem.* **1993**, *3*, 215.

(5) Eichorn, D. M.; Skee, D. C.; Broderick, W. E.; Hoffman, B. M. *Inorg. Chem.* **1993**, *32*, 491.

(6) (a) Manriquez, J. M.; Yee, G. T.; McLean, R. S.; Epstein, A. J.; Miller, J. S. *Science* **1991**, *252*, 1415. (b) Epstein, A. J.; Miller, J. S., in the Proceedings of Nobel Symp. No. NS-81; *Conjugated Polymers and Related Materials: The Interconnection of Chemical and Electronic Structure*; Oxford University Press: New York, 1993; p 475. *Chim. Ind.* **1993**, *75*, 185. (c) Miller, J. S.; Yee, G. T.; Manriquez, J. M.; Epstein, J. M., in the Proceedings of Nobel Symposium No. NS-81; *Conjugated Polymers and Related Materials: The Interconnection of Chemical and Electronic Structure*; Oxford University Press: New York, 1993; p 461. *Chim. Ind.* **1992**, *74*, 845. (d) Epstein, A. J.; Miller, J. S. *Mol. Cryst., Liq. Cryst.* **1993**, *228*, 99.

(7) Miller, J. S.; Calabrese, J. C.; McLean, R. S.; Epstein, A. J. *Adv. Mater.* **1992**, *4*, 498. Zhou, P.; Epstein, A. J.; McLean, R. S.; Miller, J. S. *J. Appl. Phys.* **1993**, *73*, 6569.

(8) McConnell, H. M. *Proc. R. A. Welch Found. Chem. Res.* **1967**, *11*, 144.

(9) Miller, J. S.; Epstein, A. J. *J. Am. Chem. Soc.* **1987**, *109*, 3850.

(10) Kollmar, C.; Kahn, O. *J. Am. Chem. Soc.* **1991**, *113*, 7987.

(11) Buchachenko, A. L. *Mol. Cryst., Liq. Cryst.* **1989**, *176*, 307.

(12) Tchougreff, A. L.; Misurkin, I. A. *Chem. Phys.* **1991**, *153*, 371. Tchougreff, A. L.; Misurkin, I. A. *Phys. Rev. B* **1992**, *46*, 5357.

(13) Kollmar, C.; Couty, M.; Kahn, O. *J. Am. Chem. Soc.* **1992**, *113*, 7994.

0002-7863/94/1516-7243$04.50/0

The detailed spin density distributions of both the donors and acceptors are critical in identifying the spin-coupling mechanism, but these distributions have not been directly measured before in the solid state. As a first step to elucidate the spin coupling mechanism we now report the determination of the spin distribution of isolated $[TCNE]^{\bullet-}$, **1**, as determined from single-crystal polarized neutron diffraction studies of $[Bu_4N]^+[TCNE]^{\bullet-}$. $[TCNE]^{\bullet-}$ is an essential component in many molecule-based magnets and an important molecule in organic chemistry. Additionally, these results extend our understanding of the spin density of organic radicals and enable the direct comparison of theoretical predictions of open-shell species with experimentally determined values.

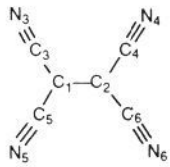

$[TCNE]^{\bullet-}$ **(1)**

Experimental Section

The spin density in a paramagnetic single crystal can be obtained from neutron scattering by aligning the spin density by means of an external magnetic field at low temperature and measuring the magnetic neutron scattering amplitudes (magnetic structure factors), F_M. Since the induced spin density is periodic, all of the measurements are made at the Bragg scattering positions. The sensitivity of the method is enhanced by the use of polarized neutrons, as the nuclear scattering (nuclear structure factors F_N) amplifies the magnetic signal.[15] The "flipping" ratio, R, of the Bragg reflections, *i.e.*, the ratio of intensities for the up ($I^\uparrow$) and down ($I^\downarrow$) polarizations of the incident beam, is measured. If the crystal structure is known, the nuclear contribution to the scattering is calculated and the magnetic information (the F_M's) is obtained from the R's by solving eq 1, where $\vec{F}_M = \hat{z}F_M$, $F_{M\perp} = F_M \cos\alpha$, $F_{M\perp_z} = F_M \cos^2\alpha$, $\hat{z}$ is the direction of the applied field, and α is the angle of the scattering vector and $\hat{z}$.

$$R = \frac{I^\uparrow}{I^\downarrow} = \frac{F_N^2 + F_{M\perp}^2 + 2F_N F_{M\perp_z}}{F_N^2 + F_{M\perp}^2 - 2F_N F_{M\perp_z}} \qquad (1)$$

The crystal structure of the compound was determined by using both X-ray and unpolarized neutron diffraction.[16] The $[TCNE]^{\bullet-}$'s are well isolated both from the cations and from each other in the crystal. As in neutral TCNE,[17] $[TCNE]^{\bullet-}$ has essentially D_{2h} symmetry as previously observed in other structures and as predicted by molecular orbital calculations.[18]

The polarized neutron measurements were performed in two series of experiments on the DN2 diffractometer at the Siloe reactor (CEA Grenoble). A 7.4 × 3.6 × 1.7 mm crystal grown by slow diffusion of diethyl ether into an acetonitrile solution of the salt was mounted in a cryomagnet and cooled down to 1.8 K in an applied field of 4.65 T. In the first experiment, the crystal was mounted with the b axis parallel to the magnetic field. In the second experiment, the crystal was rotated to align the $[10\bar{1}]$ axis collinear to the magnetic field. With both orientations, 211 independent "flipping" ratios were collected up to $\sin(\theta/\lambda) = 0.36$ Å, with the incident wavelength $\lambda = 1.205$ Å for the neutrons. There is one significant restriction in the measurements. The construction of the lifting-counter and the split-coil cryomagnet permits access only to a "slice" in reciprocal space for each mounting of the sample. For example, in the first series of experiments only the $(h0l)$, $(h1l)$, and $(h2l)$ Bragg reflections could be measured. Thus, the resolution in the vertical direction is poor. Nevertheless, the data are sufficient for the reconstruction of a projection onto the ac plane which is essentially the $[TCNE]^{\bullet-}$ molecular plane. The problem is only partly solved by mounting the crystal in the second orientation since on projection along the $[10\bar{1}]$ axis two symmetrically equivalent $[TCNE]^{\bullet-}$'s overlap. Thus, the second series of experiments does not reveal much information of the spin density distribution perpenidular the molecular plane.

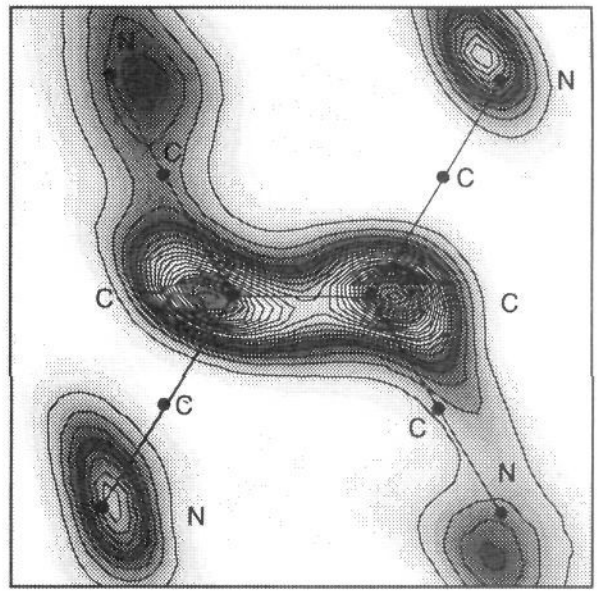

Figure 1. Maximum Entropy (MaxEnt) reconstruction of the spin density. Projection onto the $[TCNE]^{\bullet-}$ molecular (xy) plane.

Data Processing and Results

The magnetic structure factors F_M are the Fourier components of the magnetization (spin) density $S(\mathbf{r})$. Reconstruction of the spatial spin density from the experimental magnetic structure factors is a typical Inverse Fourier (IF) problem. The IF problem is solved within the limitations of the accuracy and completeness of polarized neutron diffraction data. However, the data are noisy, the error bars are uneven, the sampling of data points in reciprocal space is somewhat arbitrary, and the spatial resolution of the diffraction experiment (see above) is limited. Thus, several approaches for solving the IF problem were used.

Model-independent IF methods can be used to reconstruct the spin density without involving any *a priori* knowledge of the spin density distribution. It is important to apply such a method in order to test the models and to judge the quality of the data. The most straightforward approach to solving the IF problem is to calculate the inverse Fourier sum over all Bragg reflections for which the F_M's were determined.

$$S(x,y,z) = \sum_{h,k,l} F_M(h,k,l)^{-2\pi i(hx+ky+lz)} \qquad (2)$$

This method has been widely used to interpret polarized neutron diffraction data, but it has drawbacks due to incomplete and noisy data. Since not all of the Fourier components are known, there are many possible 3-D spin density distributions (maps) which fit the data. Fourier inversion selects the one with zero values for unmeasured coefficients. In contrast, the recently developed Maximum of Entropy (MaxEnt) technique[19-21] selects

(14) Tchougreeff, A. L.; Hoffmann, R. *J. Phys. Chem.* **1993**, *97*, 350.

(15) Gillon, B.; Schweizer, J. Study of Chemical Bonding in Molecules: The Interest of Polarized Neutron Diffraction. *Molecules in Physics, Chemistry and Biology*; Maruani, J., Ed.; Kluwer Academic Publisher: Hingham, MA, 1989; Vol. II, p 111.

(16) X-ray analysis: A 0.40 × 0.38 × 0.45 mm crystal of $[Bu_4N][TCNE]$ (MW = 370.957) was grown from Et_2O/MeCN and belongs to the monoclinic $P2_1/n$ (No. 14) space group; $a = 14.651(3)$ Å, $b = 8.446(1)$ Å, $c = 19.669(5)$ Å; $\beta = 106.21(1)°$, $V = 2337.1$ Å^3; $Z = 4$; $\rho_{calc} = 1.053$ g/cm^3; $\mu_{Mo} = 0.60$ cm^{-1}, 0.60 cm^{-1} at −70 °C. Using an Enraf-Nonius CAD4 diffractometer, 4040 reflections were measured using a graphite-monochromated Mo Kα radiation. With 244 variables, the structure was refined using 1560 data for which $I > 3\sigma(I)$ to convergence of $R = 0.049$ and $R_w = 0.046$. Neutron analysis (10 K): $a = 14.550(36)$ Å, $b = 8.263(13)$ Å, $c = 19.686(48)$ Å, $\beta = 106.1(1)°$. Becker, P.; Coppens, P.; Ross, S. K. *J. Am. Chem. Soc.* **1973**, *95*, 7604.

(18) Dixon, D. A.; Miller, J. S. *J. Am. Chem. Soc.* **1987**, *109*, 3656.

(19) Papoular, R. J.; Gillon, B. Neutron Scattering Data Analysis; Johnson, M. W., Ed. In *Inst. Phys. Conf. Ser. (Bristol)* **1993**, *107*, 101.

(20) Papoular, R. J.; Gillon, B. *Europhys. Lett.* **1990**, *13*, 429.

(21) Papoular, R. J.; Ressouche, E.; Schweizer, J.; Zheludev, A. *Fundam. Theor. Phys.* **1993**, *53*, 1993.

Table 1. Refinement Statistics and Refined Populations of [TCNE]•⁻ Atoms in μ_B[a]

	wave function refinement	multipolar expansion of the spin density
no. of variables	13	17
N_{obs}/N_{var}	16.23	12.14
χ^2 [b]	1.8	1.4
C1	0.185(7)	0.255(3)
C2	0.256(7)	0.255(3)
C3	–0.013(6)	–0.040(6)
C4	–0.012(7)	–0.030(6)
C5	–0.035(7)	–0.025(6)
C6	–0.018(7)	–0.057(7)
N3	0.096(7)	0.095(6)
N4	0.097(7)	0.094(6)
N5	0.113(7)	0.096(6)
N6	0.120(8)	0.118(6)
total spin	0.789(22)	0.761(17)

[a] Negative values correspond to excess β electrons. [b] Experimental estimated standard deviation.

among all the maps consistent with the data the most probable one, the one which maximizes the Boltzmann entropy.

$$\text{Entropy} = -\int_{\text{unit cell}} s(\bar{r}) \ln(s(\bar{r}))d^3r \text{ where}$$

$$s(\bar{r}) = \frac{S(\bar{r})}{\int_{\text{unit cell}} S(\bar{r})d^3r} \quad (3)$$

The MaxEnt technique strictly applies to positive densities, but the method can be modified to treat sign-alternating densities by considering the α- and β-spin densities as being independent. This method gives much better results than conventional Fourier inversion and is model independent. Figure 1 represents the MaxEnt reconstructed spin density projected onto the [TCNE]•⁻ molecular plane. The MaxEnt reconstruction reveals three main features of the spin density distribution. (1) All of the spin resides on the [TCNE]•⁻ anion; no spin density is detected on $[Bu_4N]^+$. (2) Within the [TCNE]•⁻ radical most of the spin is localized on the central sp²-carbon atoms. Smaller, but significant, spin densities are observed in the vicinity of the nitrogen atoms. (3) The spin density on C_1 and C_2 is not centered on these atoms, but it is shifted backwards away from the midpoint of the central C–C bond. It should be emphasized that these results are not artifacts of the data-treatment procedure, as no information concerning atomic positions or other *a priori* knowledge was used to obtain them.

An alternative approach to solve the IF problem is to use a parametrized model of the spatial spin density distribution and then refine the model parameters to fit the experimental structure factors. A good model should be flexible enough to describe the actual density with as few parameters as possible. A simple, frequently used model is based on individual atomic magnetic wave functions.[15] In this framework a Hartree–Fock type wave function, $|\varphi\rangle$, is constructed at each atomic site from standard Slater-type atomic orbitals (STO's):

$$|\varphi\rangle = \sum_j \alpha_j |\varphi_j\rangle \quad (4)$$

The j index labels the STO's and α_j are real coefficients normalized to give $\langle\varphi|\varphi\rangle = 1$. The spin density is then given by:

$$S(\mathbf{r}) = \sum_{\text{atoms}} S_i \varphi^*_i(\mathbf{r})\varphi_i(\mathbf{r}) \quad (5)$$

where S_i are the individual atomic populations. The parameters of this model are the S_i, the set of coefficients α_j for each atom, and the radial exponents of the STO's for each φ_j. Note that in this model we have squared the wave function at each site and summed the squares. This is not formally correct as we should ideally form a linear combination of the atomic wave functions and take the square of the resulting wave function, but in using eq 5 we allow for negative spin populations. This would introduce a cross-term which leads to significantly more complicated equations. Considering the available data, the additional computational effort is not justified.

Table 2. Spherical Function Population Coefficients for the Central sp²-Carbon Atoms[a]

monopole	1
dipole, x	–0.210(17)
quadrupole, z^2	0.211(89)
octupole, xz^2	–0.513(159)
octupole, x^3	0.070(125)

[a] The values are scaled to give monopolar contribution of unity.

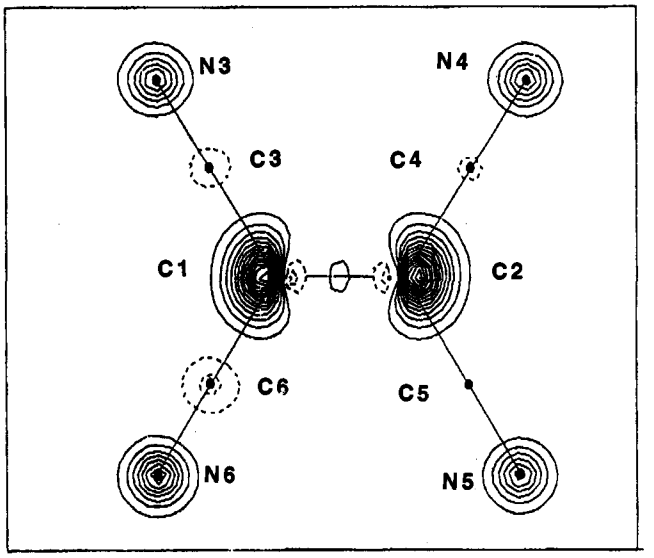

Figure 2. Spin density reconstructed by model refinement. Projection onto the [TCNE]•⁻ molecular plane.

For [TCNE]•⁻ the simplest model suggests including $|2p_z\rangle$ (where x,y is the molecular plane) orbitals for the C and N atoms into eq 4; in this model α_j is unity. The atomic spin populations and radial exponents were refined using a modification of the least-squares program MOLLY.[22] Refinement statistics, calculated spin populations, and the value of the Slater radial exponents are listed in Table 1. The results are not very satisfactory as the residual estimated standard deviation (χ^2) is too large. The refined spins on C_1 and C_2 are unequal, which is surprising as isolated [TCNE]•⁻ should have D_{2h} symmetry. This arises from the low symmetry of the monoclinic unit cell.

To understand why this simple model fails to represent the spin density distribution one has to look again at the results of the model-independent reconstruction. As noted, the MaxEnt results show strong off-centering of the spin density on the central carbon atoms. This effect is quite pronounced but it cannot be accounted for by the simple model given above which requires cylindrical symmetry of the spin density in the vicinity of all atomic centers because we use a single p_z function at each center.

It is well-known from molecular orbital theory that antibonding orbitals do not have their maximum electron density centered over the bond, but rather the density is bent away from the center of the bond due to the presence of a node. The additional electron in [TCNE]•⁻ is located in an antibonding π^* orbital and thus the spin density on C_1 and C_2 cannot be properly described by using only axially symmetrical $|p_z\rangle$ orbitals. A model permitting more freedom of the spin density shape in the vicinity of the central carbon atoms is required. A more flexible approach would be to directly model the spin density instead of the wave function. This can be accomplished by expanding the spin density around the

(22) Hansen, H. K.; Coppens, P. *Acta Crystallogr.* **1978**, *A34*, 909.

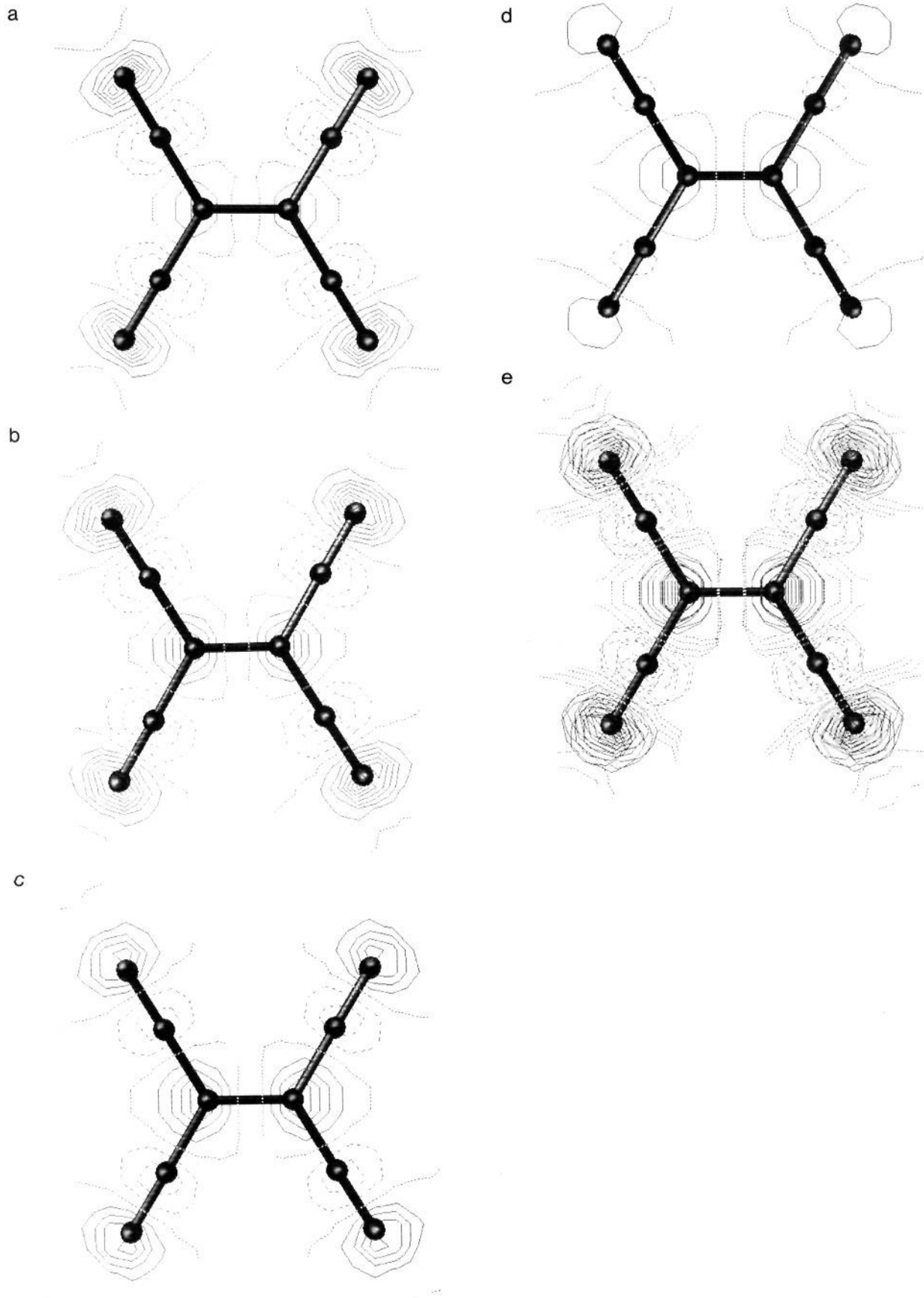

Figure 3. UHF *ab initio* spin density projected onto the $[TCNE]^{\bullet-}$ molecular (xy) plane. Spin density in sections at contour levels from –0.040 to 0.076 $e^-/Å^3$ at every 0.01 $e^-/Å^3$. The solid line is positive spin density (excess α spin) and the dashed line is negative spin density (excess β spin). Note that the spin density at the sp-Cs is negative. The dotted line is the nodal plane. The distance from the plane of the molecule is (a) 0.00, (b) 0.25, (c) 0.50, and (d) 0.75 Å. The superposition of (a) through (d) is depicted in (e).

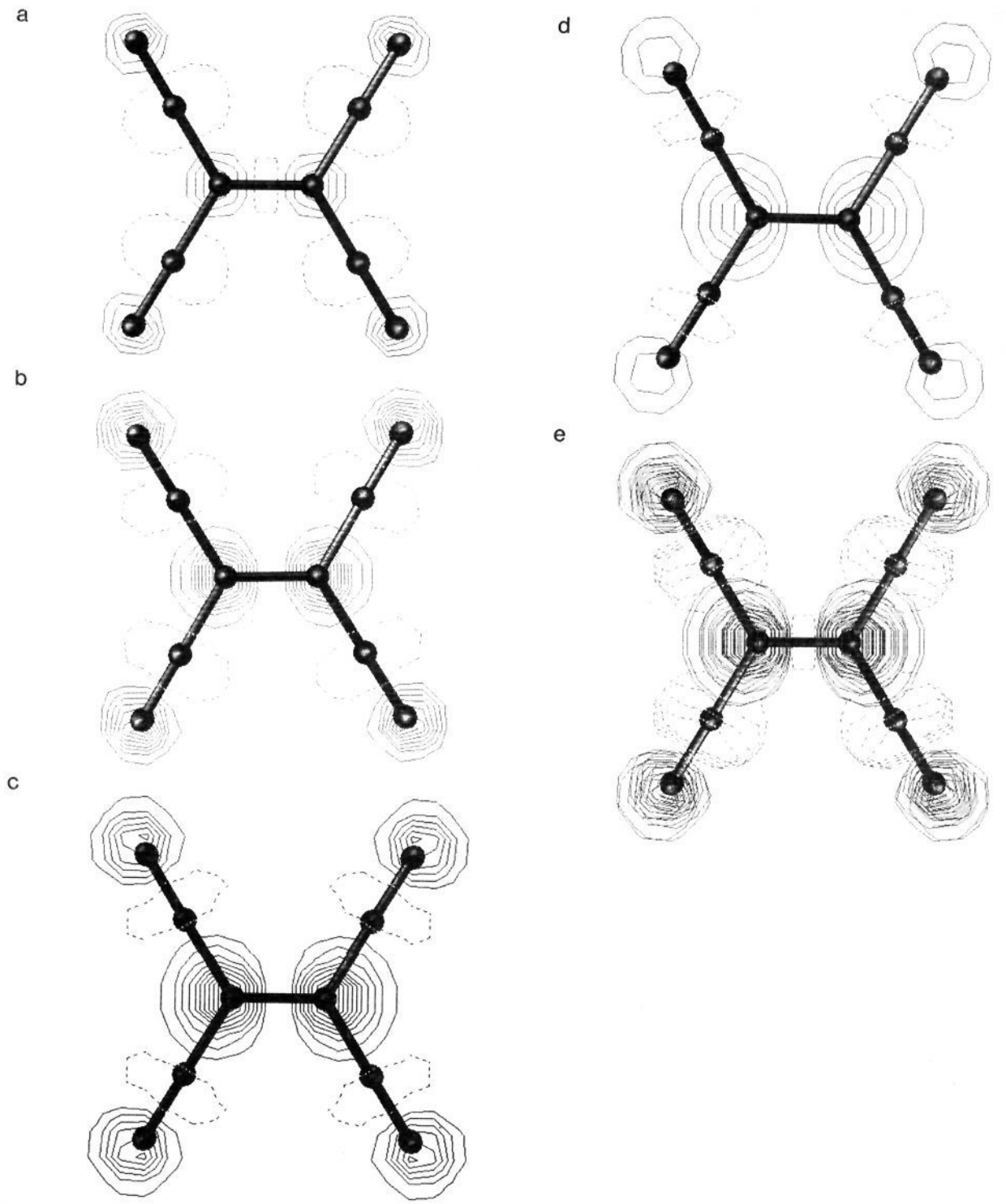

Figure 4. Nonlocal DFT spin density projected onto the [TCNE]•⁻ molecular (xy) plane. Spin density in sections at contour levels from –0.023 to 0.231 e⁻/Å³ at every 0.02 e⁻/Å³. The solid line is positive spin density (excess α spin) and the dashed line is negative spin density (excess β spin). Note that the spin density at the sp-Cs is negative. The dotted line is the nodal plane. The distance from the plane of the molecule is (a) 0.00, (b) 0.25, (c) 0.50, and (d) 0.75 Å. The superposition of (a) through (d) is depicted in (e).

nuclei into a multipolar series.[23] The spin density is now treated as a sum of real spherical harmonic functions y_l^m centered at each atomic site:

$$S(\mathbf{r}) = \sum_{\text{atoms}} \sum_{k=0}^{\infty} R_k(\mathbf{r}) \sum_{m=-l}^{l} P_l^m \, y_l^m(\hat{\mathbf{r}}) \qquad (6)$$

where P_l^m and $R_k(\mathbf{r})$ are the population coefficients and Slater type radial functions, respectively. The population coefficients as well as the Slater radial exponents are the parameters in this model.

Due to the quality and quantity of the data, it was decided that a hybrid approach should be used. The MaxEnt results clearly showed that the dominant spin density is on the two central carbons C_1 and C_2 consistent with the density functional theory (DFT) calculations reported below. In the final model only a minimal basis set of orbitals perpendicular to the molecular plane were used, the $|2p_z>$ orbitals for N_{3-6} and C_{3-6}, whereas a multipolar

(23) Brown, P. J.; Capiomont, A.; Gillon, B.; Schweizer, J. *J. Magn. Magn. Mater.* **1979**, *14*, 286.

Table 3. Comparison of Experimental Results with *ab Initio* Calculations[g]

atom	exp[a]	ROHF[c] 3-21G	UHF[b] 3-21G	UMP2[b] 3-21G	UHF[b] 6-311G*	UHF[c] DZV+(d,p)	UHF[c,d] MINI-1	UHF[c,e] STO-3G	LDFT[b] TZVP	LDFT[c] TZVP	NLDFT[c] TZVP	NLDFT[c,f] TZVP/|2p$_z$⟩	NLDFT[b] TZVP
C_1	0.33	0.34	0.51	0.52	0.48	0.61	0.54	0.49	0.28	0.28	0.29	0.25	0.30
C_2	0.33	0.34	0.56	0.55	0.50	0.61	0.54	0.49	0.28	0.28	0.29	0.25	0.29
C_3	–0.05	0.01	–0.50	–0.62	–0.40	–0.58	–0.35	–0.77	–0.02	–0.03	–0.04	–0.01	–0.04
C_4	–0.04	0.01	–0.70	–0.67	–0.60	–0.58	–0.35	–0.77	–0.03	–0.03	–0.04	–0.01	–0.05
C_5	–0.03	0.01	–0.55	–0.53	–0.46	–0.58	–0.35	–0.77	–0.03	–0.03	–0.04	–0.01	–0.04
C_6	–0.08	0.01	–0.61	–0.63	–0.54	–0.58	–0.35	–0.77	–0.03	–0.03	–0.04	–0.01	–0.05
N_3	0.12	0.07	0.49	0.50	0.42	0.52	0.23	0.79	0.13	0.14	0.15	0.13	0.14
N_4	0.12	0.07	0.69	0.70	0.60	0.52	0.23	0.79	0.15	0.14	0.15	0.13	0.16
N_5	0.13	0.07	0.53	0.52	0.44	0.52	0.23	0.79	0.14	0.14	0.15	0.13	0.14
N_6	0.16	0.07	0.60	0.51	0.53	0.52	0.23	0.79	0.13	0.14	0.15	0.13	0.15

[a] Spin population normalized to unity from the hybrid basis set approach. [b] Experimental geometry determined from neutron diffraction. [c] D_{2h} geometry of the isolated $[TCNE]^{\bullet-}$ ion. [d] Yamaguchi, K.; Okumura, M.; Kawamura, T.; Noro, T.; Nakasuji, K. *Mol. Cryst., Liq. Cryst.* **1992**, *218*, 229. [e] Dixon, D. A.; Miller, J. S. *J. Am. Chem. Soc.* **1987**, *109*, 3656. [f] $|2p_z\rangle$ component. The difference between the value in this and the previous columns is the spin population in the molecular plane $[|2s\rangle + |2p_x\rangle + |2p_y\rangle]$. [g] UHF = unrestricted Hartree–Fock; MP2 = second-order Moller–Plesset; LDFT = local density functional theory; NLDFT = nonlocal density functional theory; ROHF = restricted open-shell Hartree–Fock; DZV = double-ξ valence.

expansion of the spin density was used for the central C_1 and C_2 atoms. This multipolar expansion was truncated at $l = 3$. In order to reduce the number of adjustable parameters, maximum advantage was taken of molecular symmetry. Only those functions that are even with respect to z and y were used (with the x axis parallel to the central C–C bond). (Thus x, y, and z make an orthonormal basis set.) Furthermore, the spin densities on C_1 and C_2 were constrained to be symmetric with respect to the plane perpendicular to the central C–C bond and passing through its midpoint. The final refinement ($\chi^2 = 1.4$) results are listed in Table 1. Table 2 shows the refined population coefficients for the spherical functions on C_1 and C_2. The projection of the spin density along the z axis onto the approximate molecular plane is presented in Figure 2.

To test if the spin density on the other $[TCNE]^{\bullet-}$ atoms has the $|2p_z\rangle$ shape, preliminary refinements in which the contributions from these atoms were reduced to spherical ones were made ($\chi^2 = 1.82$). The $|2p_z\rangle$ orbital model better fits the observed densities. We also did two other sets of calculations to see if the fit could be improved. First, we enforced D_{2h} symmetry on the spin density distribution, but not on the structure of the ion. This yielded spin populations (α–β electrons) of 0.248(3), –0.035(3), and 0.110(3) μ_B for C_1, C_2, and N, respectively, with $\chi^2 = 1.5$. These are essentially the average of the values given in Table 1 with a total spin of 0.80 μ_B. As the second largest spin population is on the N, we also used a multipolar expansion for it in D_{2h} symmetry which gave populations of 0.239(4), –0.033(3), and 0.107(4) μ_B for C_1, C_2, and N, respectively, with $\chi^2 = 1.5$. Thus the results are not substantially changed from the model given above with only the sp^2 carbons being symmetrized.

The model with only the sp^2 carbons symmetrized provides the best fit to the experimental data. The greatest spin contribution (66%) is from C_1 and C_2. The contribution from the nitrogen atoms is also significant (52%), while the total spin contribution from C_3–C_6 is small (–20%) and *negative*. The multipole expansion shows that the spin density is not centered over the nuclei at the C_1 and C_2 but is bent away from the midpoint of the C_1–C_2 bond. These results are consistent with the results of the MaxEnt analysis shown in Figure 1. Note that the model fitting the experimentally data yields 0.76 μ_B, which is less than the 0.9 μ_B expected from $S = {}^1/_2$ Curie behavior. The missing spin is probably due to the limited amount of data available.

Ab Initio Calculations

Unrestricted Hartree–Fock (UHF) open shell calculations of the spin density for $[TCNE]^{\bullet-}$ were done with the 3-21G and 6-311G** basis sets at the experimental geometry.[24] We also performed calculations with the 3-21G and DZV+(d,p) basis sets[25] at a geometry optimized at the nonlocal DFT level described below. Similar results were obtained with the 3-21G basis set at the MP2 level at the experimental geometry. The MONSTERGAUSS[26] and GAUSSIAN90/90[27] programs were used for these calculations. Density functional theory, DFT,[28–32] calculations at the local and self-consistent nonlocal levels were done with a polarized triple-ζ valence (TZVP) basis set[24] with the program DGAUSS.[33–36] The calculations were done with the local potential of Wilks, Volk, and Nusair[37] and the nonlocal correlation potential of Perdew[38] and the nonlocal exchange potential of Becke.[39] The results of the *ab initio* calculations are presented in Table 3 together with literature results and our experimental results normalized to one spin per $[TCNE]^{\bullet-}$. Figure 3 shows the Hartree–Fock results, whereas the spin density at the nonlocal DFT level is shown in Figure 4.

The calculated geometry at the self-consistent nonlocal DFT level is in good agreement with the neutron diffraction determined geometry with all of the calculated distances longer than the average observed values (Table 4). The C_1–C_2 distance is calculated to be 0.019 Å longer than the observed value, but it is within two estimated standard deviations (esds). The C_1–CN distance is only 0.005 Å too long and the CN distance is 0.009

(24) Godbout, N.; Salahub, D. R.; Andzelm, J.; Wimmer, E. *Can. J. Chem.* **1992**, *70*, 560.

(25) Dunning, T. H., Jr.; Hay, P. J. In *Methods of Electronic Structure Theory*; Schaefer, H. F., III, Ed.; Plenum Press: New York, 1977; Chapter 1.

(26) MONSTERGAUSS: Peterson, M. R., Poirier, R. A.; Department of Chemistry, University Toronto, Toronto, Canada.

(27) GAUSSIAN92: Frisch, M. J., Trucks, G. W., Head-Gordon, M., Gill, P. M. W., Wong, M. W., Foresman, J. B., Johnson, B. G., Schlegel, H. B., Robb, M. A., Replogle, E. S., Gomperts, R., Andres, J. L., Raghavachari, K., Binkley, J. S., Gonzalez, C., Martin, R. L., Fox, D. J., DeFrees, D. J., Baker, J., Stewart, J. J. P., Pople, J. A.; Gaussian Inc.: Pittsburgh, PA, 1992.

(28) Parr, R. G.; Yang, W. *Density Functional Theory of Atoms and Molecules*; Oxford University Press: New York, 1989.

(29) Salahub, D. R. In *Ab Initio Methods in Quantum Chemistry-II*; Lawley, K. P. J., Ed.; Wiley & Sons: New York, 1987; p 447.

(30) Wimmer, E.; Freeman, A. J.; Fu, C.-L.; Cao, P.-L.; Chou, S.-H.; Delley, B. In *Supercomputer Research in Chemistry and Chemical Engineering*; Jensen, K. F., Truhlar, D. G., Eds.; ACS Symp. Ser. No. 353; American Chemical Society: Washington, DC, 1987; p 49.

(31) Jones, R. O.; Gunnarsson, O. *Rev. Mod. Phys.* **1989**, *61*, 689.

(32) Zeigler, T. *Chem. Rev.* **1991**, *91*, 651.

(33) Andzelm, J.; Wimmer, E.; Salahub, D. R. In *The Challenge of d and f Electrons: Theory and Computation*; Salahub, D. R., Zerner, M. C., Eds.; ACS Symp. Ser. No. 394; American Chemical Society: Washington, DC, 1989; p 228.

(34) Andzelm, J. W. In *Density Functional Methods in Chemistry*; Labanowski, J., Andzelm, J. W., Eds.; Springer-Verlag: New York, 1991: p 101.

(35) Andzelm, J. W.; Wimmer, E. *J. Chem. Phys.* **1992**, *96*, 1280.

(36) DGAUSS is a local density functional program available via the Cray Unichem Project.

(37) Vosko, S. J.; Wilk, L.; Nusair, M. *Can J. Phys.* **1980**, *58*, 1200.

(38) Perdew, J. P. *Phys. Rev. B* **1986**, *33*, 8822.

(39) Becke, A. D. *Phys. Rev. A* **1988**, *38*, 3098. Becke, A. D. In *The Challenge of d and f Electrons: Theory and Computation*; Salahub, D. R., Zerner, M. C., Eds.; ACS Symp. Ser. No. 394; American Chemical Society: Washington, DC, 1989; p 166. Becke, A. D. *Int. J. Quantum Chem. Quantum Chem. Symp.* **1989**, *23*, 599.

Table 4. Experimental and Calculated Geometry Parameters for [TCNE]•⁻ [a]

parameter	calc[b]	expt	parameter	calc	expt
$r(C_1–C_2)$	1.448	1.429(8)	$(C_3–C_1–C_6)$	117.4	118.1(6)
$r(C_1–C_3)$	1.411	1.406(9)			119.0(6)
		1.393(9)	$(C_1–C_3–N_3)$	179.8	179.8(7)
		1.419(9)			178.2(7)
		1.405(9)			178.6(8)
$r(C_3–N_3)$	1.179	1.157(7)			179.2(7)
		1.181(8)			
		1.164(7)			
		1.177(7)			

[a] Bond distances in Å. Bond angles in deg. [b] Calculation done at the nonlocal DFT level with a triple-ξ valence polarized (TZVP) basis set.

Å too long. The NC–C_1–CN angle is calculated to be smaller than the experimental angle by 1.6° and the calculated value for the C_1–C–N bond angle is slightly more linear than the average experimental value. The calculated structure is in reasonable agreement with the structure obtained at the UHF level with the STO-3G basis set.

Discussion

The averaged experimental sp^2-C, sp-C, and N atomic spin populations are respectively 33%, –5%, and 13% of the total spin of the radical assuming the missing spin can be apportioned to the various atoms in the anion. All of the *ab initio* calculations predict the same signs for the spin populations as observed in our experiments. The ordering of the magnitudes of the spins is consistent with previous estimates based on ESR spectroscopy and molecular orbital models.[40] As opposed to the molecular orbital-based methods which exaggerate the negative spin on the sp-C's and the spin populations on the N's, the DFT calculations correctly predict the magnitudes of the atomic spin populations. These results confirm that the singly occupied (magnetic) molecular orbital of the [TCNE]•⁻ radical is the π^* orbital.

The calculations show additional interesting features. From the results of the DFT calculations we predict that most of the spin is localized in the $|2p_z>$ orbitals. The smallest percent contribution of the $|2p_z>$ is found for the sp carbons consistent with the differences in the EPR measurements. The ROHF/3-21G calculation provides further information about the spin density. The ROHF results are very similar for the sp^2 carbons as compared to the DFT results. The ROHF results clearly show that the excess β-spin on the sp carbons found in the spin unrestricted calculations is due to a spin polarization of the in-plane π orbitals of the cyano group. Clearly the UHF spin densities exaggerate the spin polarization of the cyano group. The ROHF spin densities also provide insight into how the spin density is partitioned. The actual spin density values on C_1 and C_2 are 0.54 for the diagonal value and –0.20 for the off-diagonal element coupling C_1 and C_2. It is not surprising that the spin polarization is exaggerated at the UHF/MO level as the value of S^2 [$S^2 = S(S+1)$ where S is the total spin] shows significant spin contamination. For example, values of S^2 are 1.084 (3-31G) and 1.065 (DZV+d) as compared to a value of 0.75 for $S = {}^1/_2$.

The spin density on C_1 and C_2 is bent away from the midpoint of the C_1–C_2 bond consistent with the antibonding character of the SOMO. This effect is unambiguously detected by modeling the spin density and by the model-independent approach. This can be clearly seen in the spin density calculated by the DFT method, Figure 4, and in the plot of the SOMO, Figure 5.

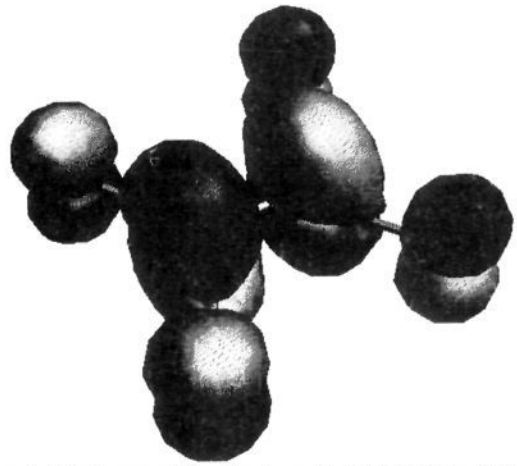

Figure 5. Singly occupied molecular orbital (SOMO) for [TCNE]•⁻ (nonlocal DFT calculation at an 0.10 contour level).

Conclusion

Polarized neutron diffraction is presently the most powerful tool for determining the absolute spin density of a radical. In contrast to resonance techniques, it can be used to determine the shape of the spin density and the total spin populations. The results show that the excess α-spin on the [TCNE]•⁻ is not completely localized on the sp^2-C's but is distributed across the radical as it has significant contributions from the nitrogens. This is important as it demonstrates that [TCNE]•⁻ with either a cofacial nonbonded {as for example in $[Fe(C_5Me_5)_2][TCNE]$} or covalently bonded {as for example in [MnTPP][TCNE] and $V[TCNE]_x{\cdot}yCH_2Cl_2$} arrangement has the possibility for strong magnetic interactions with neighboring spin sites. The spin is predominantly on the out-of-plane $|p_z>$ orbitals. Studies on $[Fe(C_5Me_5)_2]^{\bullet+}$ and $[Fe(C_5Me_5)_2][TCNE]$ are in progress. The various spin unrestricted *ab initio* methods do predict the correct signs of the spin populations; however, only the DFT method can predict the magnitude for the spin populations for these treatments based on a single configuration wave function. The combination of sophisticated experimental and theoretical techniques as described here will help to provide the basis for a better understanding of molecule-based magnetism.

Acknowledgment. The authors gratefully acknowledge the support that the Department of Energy, Division of Materials Sciences (Grant Nos. DE-FG02-86BR45271 and DE-FG03-93ER45504) has given to enable these studies and the single-crystal X-ray analysis provided by Carlos Vazquez, William J. Marshall, and Joseph C. Calabrese.

Supplementary Material Available: Tables of X-ray crystallographic data, fractional coordinates, anisotropic thermal parameters, interatomic distances, and intramolecular angles and nonbonding distances (11 pages); listing of structure factors (2 pages). This material is contained in many libraries on microfiche, immediately follows this article in the microfilm version of the journal, and can be ordered from the ACS; see any current masthead page for ordering information.

(40) Kaplan, M. L.; Haddon, R. C.; Bramwell, F. B.; Wudl, F.; Marshall, J. H.; Cowan, D. O.; Gronowitz, S. *J. Phys. Chem.* **1980**, *84*, 427. Phillips, W. D.; Rowell, J. C.; Weissman, S. I. *J. Chem. Phys.* **1960**, *33*, 626.